

Phase Diagram of the Su-Schrieffer-Heeger-Hubbard model on a square lattice

Chunhan Feng,¹ Bo Xing,² Dario Poletti,^{2,3} Richard Scalettar,¹ and George Batrouni^{4,5,6,7}

¹*Department of Physics, University of California, Davis, CA 95616, USA*

²*Science, Mathematics and Technology Cluster, Singapore University of Technology and Design, 8 Somapah Road, 487372 Singapore*

³*Engineering Product Development Pillar, Singapore University of Technology and Design, 8 Somapah Road, 487372 Singapore*

⁴*Université Côte d'Azur, CNRS, Institut de Physique de Nice (INPHYNI), 06000 Nice, France*

⁵*Centre for Quantum Technologies, National University of Singapore; 2 Science Drive 3 Singapore 117542*

⁶*Department of Physics, National University of Singapore, 2 Science Drive 3, 117542 Singapore*

⁷*Beijing Computational Science Research Center, Beijing 100193, China*

(Dated: March 9, 2022)

The Hubbard and Su-Schrieffer-Heeger Hamiltonians (SSH) are iconic models for understanding the qualitative effects of electron-electron and electron-phonon interactions respectively. In the two-dimensional square lattice Hubbard model at half filling, the on-site Coulomb repulsion, U , between up and down electrons induces antiferromagnetic (AF) order and a Mott insulating phase. On the other hand, for the SSH model, there is an AF phase when the electron-phonon coupling λ is less than a critical value λ_c and a bond order wave when $\lambda > \lambda_c$. In this work, we perform numerical studies on the square lattice optical Su-Schrieffer-Heeger-Hubbard Hamiltonian (SSHH), which combines both interactions. We use the determinant quantum Monte Carlo (DQMC) method which does not suffer from the fermionic sign problem at half filling. We map out the phase diagram and find that it exhibits a direct first-order transition between an antiferromagnetic phase and a bond-ordered wave as λ increases. The AF phase is characterized by two different regions. At smaller λ the behavior is similar to that of the pure Hubbard model; the other region, while maintaining long range AF order, exhibits larger kinetic energies and double occupancy, *i.e.* larger quantum fluctuations, similar to the AF phase found in the pure SSH model.

Introduction: Electron-electron and electron-phonon interactions play important roles in determining the ground state properties of many-body systems. Over the past decades, much computational effort has been put into studying systems that feature one or the other of these interactions. One of the most widely used models to study the effect of electron-electron interaction with on-site repulsion U is the Hubbard model [1] which exhibits metallic, ferromagnetic, antiferromagnetic (AF) and superconducting (SC) orders, as well as intricate inhomogeneous spin and charge patterns, depending on U and the doping [2, 3]. The physics of the square lattice Hubbard model bears remarkable resemblance to that of the cuprate superconductors. Two of the most commonly studied electron-phonon Hamiltonians are the Holstein [4] and the Su-Schrieffer-Heeger (SSH) [5] models. Their fundamental difference is that in the former, electrons and phonons interact on a single site, while in the latter, the electron-phonon interactions occur on the bonds, *i.e.* in the tunneling term. The Holstein interaction is widely used to explore polaron and charge-density wave (CDW) physics [6–17], and conventional s -wave SC transitions [15, 18], while the SSH interaction occurs in systems like conjugate polymers [19], organic charge transfer salts [20], metal salts [21] and CuGeO₃ [22].

In the two-dimensional square lattice, the half-filled Holstein model predicts the emergence of a CDW phase at any value of the electron-phonon interaction λ [23]. In the presence of an additional on-site electron-electron

repulsion U , the system can exhibit dominant AF or CDW correlations depending on the relative magnitude of U and λ [24, 25]. Interestingly, there are indications of an intermediate metallic phase between the AF and CDW phases [26–29], as well as other exotic regimes [30].

For the 2D square lattice SSH model at half-filling, it was shown [31] that a finite critical electron-phonon interaction, λ_c , is needed to establish the bond-order-wave (BOW) phase, and weak antiferromagnetism was detected [32, 33] for $\lambda < \lambda_c$ despite the absence of U . In the dilute limit, where bipolarons are expected to condense into a superfluid at very high temperatures, AF is revealed as well in the effective Hamiltonian [34]. The cause of this antiferromagnetism is that, on a given bond, only electrons of different spin can tunnel simultaneously, resulting in a lowering of the energy via the electron-phonon coupling on the bonds and an *increase* in the magnitude of the kinetic energy. In contrast, in the Hubbard model at half-filling, AF order emerges in a two-step process in which U first suppresses doubly occupied sites, and then AF order occurs due to a small remnant exchange process $J \sim 4t^2/U$. The AF phase in the Hubbard limit is thereby accompanied by low kinetic energy. This distinction will play a role in a cross-over behavior we observe in the Su-Schrieffer-Heeger-Hubbard (SSHH) phase diagram.

We study here the rich interplay of BOW and AF regimes in the SSHH model. Crucially, since the phonons couple to the electrons via the kinetic term, particle-hole symmetry is preserved and there is no sign problem (SP)

at half-filling. This allows us to use determinant quantum Monte Carlo (DQMC) to study systems up to 12×12 in size and at very low temperature. This contrasts with the Hubbard-Holstein model, where the SP precludes crossing the CDW-AF phase boundary[29]. Our resulting phase diagram (Fig. 1) exposes phases of long range AF and BOW order. Prior to our work, only the quantum critical point along the $U = 0$ axis (the SSH Hamiltonian) had been determined[31]. A central observation of this work is that there are, within the AF phase, distinct regimes at small and intermediate electron-phonon coupling λ . The AF structure factor, double occupancy and kinetic energy remain almost constant for small λ . However, for larger λ these quantities show a marked dependence on λ . As a consequence, we will argue that the competition between λ and U results not only in the expected AF-BOW transition, but also in a novel crossover *within* the AF phase. This crossover is clearly signaled in the AF correlations themselves, and also in the double occupancy, kinetic energy and pairing structure factors. These changes result from competition of the localizing effect of the Hubbard term and the quantum fluctuations favored by the SSH term, although they both can lead to AF.

Model and method: We study the square lattice optical SSHH model, where the electronic hopping is modulated by an electron-phonon interaction and an on-site Coulomb repulsion is present. The Hamiltonian is

$$\begin{aligned} \mathcal{H} = & -t \sum_{\langle i,j \rangle, \sigma} \left(1 - \lambda \hat{X}_{ij} \right) \left(\hat{c}_{i\sigma}^\dagger \hat{c}_{j\sigma} + \text{h.c.} \right) - \mu \sum_{i, \sigma} \hat{n}_{i\sigma} \\ & + \sum_{\langle i,j \rangle} \left(\frac{1}{2M} \hat{P}_{ij}^2 + \frac{M}{2} \omega_0^2 \hat{X}_{ij}^2 \right) \\ & + U \sum_i \left(\hat{n}_{i\uparrow} - \frac{1}{2} \right) \left(\hat{n}_{i\downarrow} - \frac{1}{2} \right), \end{aligned} \quad (1)$$

where $\hat{c}_{i\sigma}$ ($\hat{c}_{i\sigma}^\dagger$) destroys (creates) an electron of spin $\sigma = \uparrow, \downarrow$ on site i , μ is the electron chemical potential, M is the phonon mass and ω_0 the oscillation frequency. The bond phonon displacement operator \hat{X}_{ij} connects nearest neighbor sites $\langle i, j \rangle$; its conjugate bond momentum is \hat{P}_{ij} . In the following, the magnitude of electron phonon coupling is given by the dimensionless parameter $g = \lambda / \sqrt{2M\omega_0/\hbar}$, so that the coupling term is $tg(\hat{b}_{ij} + \hat{b}_{ij}^\dagger)(\hat{c}_{i\sigma}^\dagger \hat{c}_{j\sigma} + \text{h.c.})$. The on-site Coulomb repulsion is U/t , and $\hat{n}_{i\sigma} = \hat{c}_{i\sigma}^\dagger \hat{c}_{i\sigma}$ is the number operator on site i . We work in units for which $\hbar = t = M = 1$ and fix $\omega_0 = 1$.

The Hubbard-Stratonovich (HS) transformation is used in DQMC [23, 35–37], to express the quartic Coulomb interaction in quadratic form [38, 39]. The fermions are integrated out, yielding a determinant of a matrix that has dimension of the number of spatial sites N . The entries of the matrix depend on the HS and phonon fields. We focus on half-filling ($\mu = 0$), which

does not present a SP, and work with $\beta = L_\tau \Delta\tau = 16$, where $L_\tau \sim 320$ is the number of imaginary slices, and $\Delta\tau$ is the imaginary time step. This β is sufficiently large to access the ground state of the SSH model on the lattice sizes under investigation here [31].

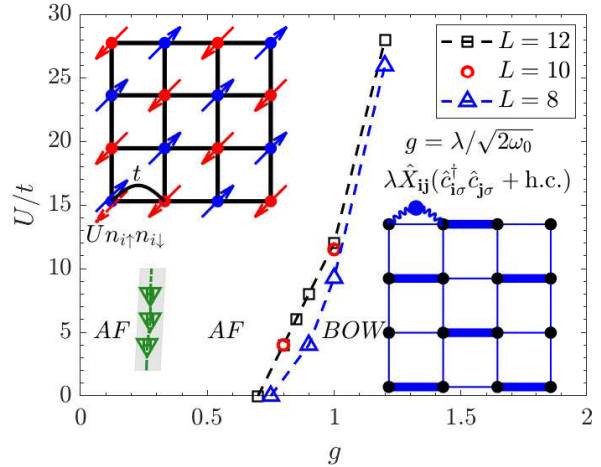


FIG. 1. Phase diagram of the SSHH model at half-filling. g is the dimensionless electron-phonon coupling constant, and U/t is the Coulomb repulsion strength. A dotted (green) line shows the location of a crossover in the nature of the AF. $\beta = 16$ ensures the system is close to the ground state for all three lattice sizes. The AF-BOW transitions for $L = 10, 12$ coincide, indicating negligible finite size effects. The insets show schematically the AF and BOW phases.

To characterize the emerging phases, we calculate the average kinetic energy in the x and y directions, $\langle K_{x(y)} \rangle = \langle \hat{c}_{i,\sigma}^\dagger \hat{c}_{i+\hat{x}(y),\sigma} + \text{h.c.} \rangle$, and the average phonon displacement in the x and y directions, $\langle X_{x(y)} \rangle$. These give insight into the broken x - y symmetry in the BOW phase. We also study the antiferromagnetic, $\langle S_i^x S_{i+r}^x \rangle$, and the bond order correlation functions, $\langle K_{x(y)}(i) K_{x(y)}(i+r) \rangle$. Their Fourier transforms, S_{AF} and $S_{K_{x(y)}}$, are respectively the AF and BOW structure factors. In addition, we examine the double occupancy, $D = \langle \hat{n}_{i\uparrow} \hat{n}_{i\downarrow} \rangle$ and the total kinetic energy $\langle K \rangle = \langle K_x \rangle + \langle K_y \rangle$ which provide additional important insight.

Results: It is well known[40, 41] that, at half filling, the square lattice Hubbard model, Eq.(1) with $\lambda = 0$, exhibits an AF phase for any $U > 0$. Similarly, it was recently established[32, 33] that the two-dimensional SSH model, Eq.(1) with $U = 0$, exhibits, at low temperature, an AF phase for small λ and a BOW[31] when λ exceeds a critical value. Here we address the unknown structure of the phase diagram in the $(g, U/t)$ plane.

To this end, we determine the phase boundaries with vertical and horizontal cuts, *i.e.* by fixing g (U/t) and studying the behavior of the system as U/t (g) is changed. The AF and BOW phases are revealed by their respective structure factors, S_{AF} and $S_{K_x}(\pi, \pi)$. For low

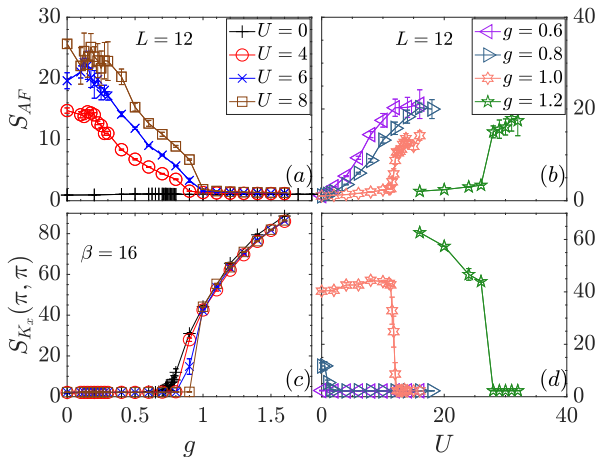


FIG. 2. DQMC results of the AF (BOW) structure factor S_{AF} ($S_{K_x}(\pi, \pi)$) for horizontal (left) and vertical (right) cuts in the phase diagram. In the AF phase, S_{AF} is finite and $S_{K_x}(\pi, \pi)$ is negligible. In the BOW phase, S_{AF} is negligible and $S_{K_x}(\pi, \pi)$ is finite.

temperature and large systems, we start simulations with a phonon configuration that favors the BOW phase in the x direction (bottom right inset Fig. 1) because this structure is found to melt rapidly in the AF phase, but takes a long equilibration time to form. We measure $S_{K_{x(y)}}(k_x, k_y)$ for all momenta and observe a peak only at $S_{K_x}(\pi, \pi)$ when the system is in the BOW phase (see more details in [42]). Comparison of data for $L = 10, 12$ indicate negligible finite size effects.

Figure 2(a,c) shows the structure factors versus the dimensionless g for several fixed values of U/t . For $U/t = 4, 6, 8$ the system is a Hubbard AF for $g = 0$, and remains AF as g increases up to a critical value, $g_c(U/t)$. For $g < g_c$, S_{K_x} is small, indicating the absence of BOW. S_{K_x} then rises rapidly upon entry into the BOW phase at $g > g_c$.

The behavior of the AF structure factor S_{AF} is more subtle. It is nonzero for $g < g_c$, but there is an appreciable change in behavior well *before* its value drops precipitously: S_{AF} is initially constant for small g , Fig. 2(a), but starts decreasing at $g_* \approx 0.2$. A finite size scaling analysis [42] shows that AF regions exhibiting true long range order on both sides of g_* . The difference between these two AF regions, inferred from the kinetic energy and double occupancy will be discussed below. Indeed, since data for structure factors are more noisy than local correlation functions, these complementary observables will present additional compelling evidence for the crossover behavior at g_* .

Returning to the AF-BOW transition with increasing g , we see, Fig. 2(a), that when S_{AF} drops, S_{K_x} becomes nonzero. This occurs at $g_c \sim 1$ for $L = 12$. In Fig. 2(b,d) we show the same quantities as panels (a,c) but now g

is fixed and U/t varies. For $g = 0.6$, S_{K_x} is small for all U/t while S_{AF} increases smoothly as U/t increases. For this value of g the system is always AF. For $g \geq 0.8$, S_{AF} is very small (essentially zero) while S_{K_x} is large up to a g -dependent critical value, $U_c(g)$, indicating that the system is in the BOW phase [31]. At $U_c(g)$, there is a first order transition from the BOW to the AF phase, with clear discontinuous jumps in the order parameters. This first order character is also observed for the larger U values in the horizontal cuts (sweeping g at fixed U) in Fig. 2(a,c).

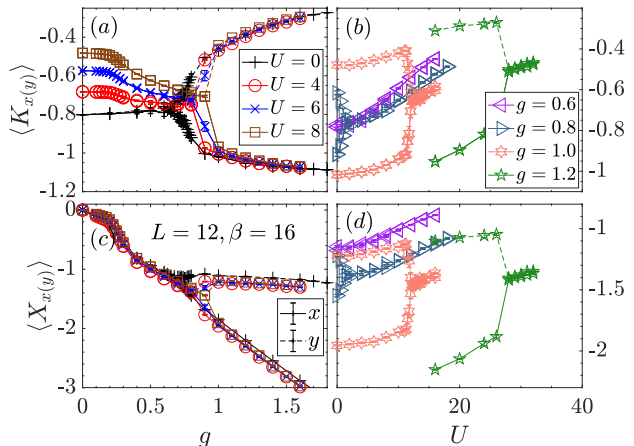


FIG. 3. DQMC results of average kinetic energy, $\langle K_{x(y)} \rangle$, and average phonon displacement, $\langle X_{x(y)} \rangle$, in x and y directions for horizontal (left) and vertical (right) cuts in the phase diagram.

As shown in Ref. [31], the BOW has (π, π) ordering vector either in x or in y with two sublattice possibilities in each direction, resulting in the Z_4 symmetry breaking (in the thermodynamic limit). We now focus on this symmetry breaking as the system leaves the AF phase and enters the BOW phase. In the AF phase, the average kinetic energy and phonon displacement in the x and y directions are equal. In the BOW phase, the average kinetic energy and phonon displacement which align with the BOW direction increase in magnitude. We show in Fig. 3 the behavior of these quantities for the same parameters as in Fig. 2. In panels (a,c), the x - y symmetry is preserved in the AF phase, $g < g_c(U)$, and broken immediately when the system enters the BOW phase. This is clearly seen in the bifurcation in $K_{x(y)}$ and $X_{x(y)}$ at g_c . As the on-site interaction becomes stronger, the electron-phonon coupling strength required to establish the BOW phase becomes larger.

In Fig. 3(b,d), for constant g , the x - y symmetry is broken for $U < U_c(g)$, $g \geq 0.8$ and restored immediately when the system exits the BOW and enters the AF phase at $U_c(g)$. For $g = 0.6$, the system is never in the BOW phase for all U and therefore the x - y symmetry is always

preserved. The values of $g_c(U)$ and $U_c(g)$ obtained in Fig. 2 and Fig. 3 are in close agreement. We remark that, as observed in both figures, a small increase in g (i.e. from 1.0 to 1.2) leads to significant changes of U_c (i.e. 12 to 26). Putting these cuts at constant g and U together yields the phase diagram shown in Fig. 1.

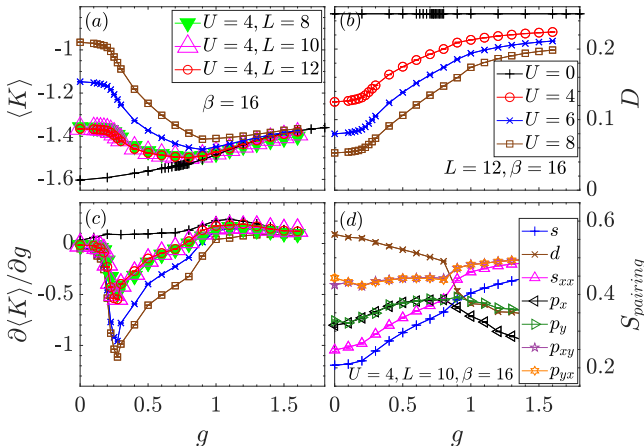


FIG. 4. (a) Average kinetic energy. (b) double occupancy for different U and fixed lattice size $L = 12$; (c) derivative of the kinetic energy with respect to g . The legends in panels (a,b) explain the symbols in panels (a,b,c). (d) pairing structure factors at fixed $U = 4$ and $L = 10$.

We now focus on the two AF regions (separated by the vertical dotted line in Fig. 1) for which S_{AF} provided initial evidence. We recall that for $g = 0$, the system is in the Hubbard AF phase for any $U > 0$, while for $U = 0$, the system is in the SSH AF phase [32, 33] for small g . The SSH AF at $U = 0$ clearly has a different mechanism from the traditional two step Hubbard model process of moment formation at energy scale U followed by moment ordering at energy scale $J \sim 4t^2/U$. A close analysis of Fig. 3(a,c) shows that both $\langle K_{x(y)} \rangle$ and $\langle X_{x(y)} \rangle$ remain almost constant for $g \lesssim 0.2$ and then increase in magnitude for $g > 0.2$. Similarly, the AF structure factor in Fig. 2(a) is approximately constant for $g \lesssim 0.2$ and decreases for larger values of g .

In Fig. 4(a), we show the average kinetic energy as a function of g for several values of U . $\langle K \rangle$ clearly exhibits a change of behavior at $g_* \approx 0.2$, supporting what is seen in Fig. 2 for S_{AF} . This is captured even more effectively in Fig. 4(c), which shows a sharp peak at $g \sim 0.275$ in $\partial \langle K \rangle / \partial g$ vs g . A comparison between $\langle K \rangle$ given in this SSHH Hamiltonian and in an (approximate) ‘effective’ Hubbard model [42] gives more insight on this crossover. Figure 4(b) shows the double occupancy, D , which increases in value for $g \gtrsim 0.2$. This behavior (larger kinetic energy and double occupancy) indicate that the system has left the “large U ” Hubbard AF, where both quantities are suppressed, and entered an AF

region strongly influenced by the SSH electron-phonon coupling, where quantum fluctuations are large. Going from one of these AF regions to the other is a crossover, not a phase transition. Nevertheless, there is a clear signature in the increased quantum fluctuations.

Since the pure SSH Hamiltonian preserves $O(4)$ symmetry, and an AF/CDW/SC degenerate ground state is expected in the anti-adiabatic limit [32, 33], it is useful to examine the superconducting structure factor S_{pairing} , the spatial sums of the real space correlations $\langle \Delta_\alpha^\dagger(i+r)\Delta_\alpha^\dagger(i) \rangle$ with standard conventions $\Delta_s^\dagger(i) = c_{i\uparrow}^\dagger c_{i\downarrow}^\dagger$, $\Delta_d^\dagger(i) = c_{i\uparrow}^\dagger \frac{1}{2}(c_{i+x\downarrow}^\dagger - c_{i+y\downarrow}^\dagger + c_{i-x\downarrow}^\dagger - c_{i-y\downarrow}^\dagger)$, etc. [43]. These are shown in Fig. 4(d). Similar changes are observed at the crossover. A bifurcation in pairing with p_x and p_y symmetry, as well as the sharp change in d , and s_{xx} pair form factors, at $g_c \sim 0.9$ also signal the AF-BOW phase transition. An interesting, and intuitively reasonable, observation is that a BOW pattern formed along the x or y -direction of the square lattice, increases pairing along plaquette diagonals (p_{xy} , p_{yx} , and s_{xx}), but competes with pairing channels which are also aligned directly along the bonds (d , p_x , p_y).

Conclusions: In this work, we used DQMC simulations to map out the phase diagram of the single orbital square lattice optical SSHH model. Our work fills in the full two dimensional phase diagram in the plane of positive U and g , hitherto only investigated along the $U = 0$ and $g = 0$ axes. The phase diagram is characterized by BOW and AF phases. At larger electron-phonon coupling strength, the x - y symmetry is spontaneously broken and the system develops a BOW with a (π, π) order. Given the different broken symmetries in the BOW and AF phases, and the sharp increase of BOW structure factor, the results indicate a first-order transition between these two phases. The most salient feature is that the ground state phase transition is much more sensitive to changes in electron-phonon coupling compared to variations in the Coulomb repulsion. We interpret this as the result of the lack of a direct competition between the two ordered phases. In the Hubbard-Holstein model, U suppresses double occupancy while the Holstein g enhances it. Thus the two interactions always conflict: they want the most fundamental structure, the site occupations, to behave completely differently yielding $U_c \sim g^2$ (at $\omega_0 = 1$). No such competition appears in the SSHH model. Indeed, both interactions individually give rise to AF order leading to somewhat cooperative tendencies. We thus argue that this is why adding U does not significantly inhibit the formation of the BOW phase by the SSH phonons, leading to a near vertical phase boundary.

In the AF region, for small electron-phonon coupling g , all the quantities that we analyzed, e.g. the AF structure factor, kinetic energy, phonon displacement and double occupancy, remain approximately constant. For $g \gtrsim 0.2$, the double occupancy and the magnitude of the kinetic energy start increasing, while the AF structure factor

decreases. This occurs even though the system still possesses true long range AF order as demonstrated by a finite size scaling analysis [42]. This is due to the fact that the Hubbard AF and the SSH AF mechanisms are different [32, 33]. This new insight into the physics of the SSH-Hubbard Hamiltonian can be thought of as analogous to the well-established crossover from Slater insulator to Mott-Hubbard insulator and from itinerant AF to Heisenberg AF with increasing U in the Hubbard model ($g = 0$) [41, 44, 45]. We focused here on intermediate to strong coupling, i.e. U exceeding half the bandwidth $W = 8t$ and $\omega_0 = t$. Further investigation of the effect of ω_0 on the cross-over is of interest.

Individually, the Hubbard and SSH Hamiltonians exhibit a rich panoply of phenomena when doped away from half-filling. The interaction U leads to a complex mixture of pseudogap physics, strange metal behavior, stripe order and d -wave pairing when doped. The SSH model hosts polarons in the dilute limit which can bind to bipolarons and condense into superconducting phases. New phases of matter are thus likely to emerge from the study of regimes of the SSHH Hamiltonian away from half-filling. Work in this direction has already begun as shown in [46].

Acknowledgments: We acknowledge fruitful discussions with W.-T. Chiu and B. Cohen-Stead. CHF and RTS are supported by the grant DOE DE-SC0014671 funded by the U.S. Department of Energy, Office of Science. D.P. acknowledges support from the Singapore Ministry of Education, Singapore Academic Research Fund Tier-II (Project No. MOE2018-T2-2-142). The computational work for this Letter was performed on resources of the National Supercomputing Centre, Singapore (NSCC) [47].

-
- [1] J. Hubbard, “Electron Correlations in Narrow Energy Bands,” *Proceedings of the Royal Society of London. Series A, Mathematical and Physical Sciences* **276**, 238–257 (1963).
- [2] A. Georges, G. Kotliar, W. Krauth, and M.J Rozenberg, “Dynamical mean-field theory of strongly correlated fermion systems and the limit of infinite dimensions,” *Rev. Mod. Phys.* **68**, 13 (1996).
- [3] Patrick A. Lee, Naoto Nagaosa, and Xiao-Gang Wen, “Doping a Mott insulator: Physics of high-temperature superconductivity,” *Rev. Mod. Phys.* **78**, 17–85 (2006).
- [4] T Holstein, “Studies of polaron motion: Part I. The molecular-crystal model,” *Annals of Physics* **8**, 325 (1959).
- [5] W. P. Su, J. R. Schrieffer, and A. J. Heeger, “Solitons in Polyacetylene,” *Phys. Rev. Lett.* **42**, 1698–1701 (1979).
- [6] R. M. Noack, D. J. Scalapino, and R. T. Scalettar, “Charge-density-wave and pairing susceptibilities in a two-dimensional electron-phonon model,” *Phys. Rev. Lett.* **66**, 778–781 (1991).
- [7] M. Vekić, R. M. Noack, and S. R. White, “Charge-density waves versus superconductivity in the Holstein model with next-nearest-neighbor hopping,” *Phys. Rev. B* **46**, 271–278 (1992).
- [8] Y.-X. Zhang, W.-T. Chiu, N. C. Costa, G. G. Batrouni, and R. T. Scalettar, “Charge order in the Holstein model on a honeycomb lattice,” *Phys. Rev. Lett.* **122**, 077602 (2019).
- [9] Chuang Chen, Xiao Yan Xu, Zi Yang Meng, and Martin Hohenadler, “Charge-density-wave transitions of Dirac fermions coupled to phonons,” *Phys. Rev. Lett.* **122**, 077601 (2019).
- [10] Chunhan Feng, Huaiming Guo, and Richard T. Scalettar, “Charge density waves on a half-filled decorated honeycomb lattice,” *Phys. Rev. B* **101**, 205103 (2020).
- [11] Manuel Weber and Martin Hohenadler, “Two-dimensional Holstein-Hubbard model: Critical temperature, Ising universality, and bipolaron liquid,” *Phys. Rev. B* **98**, 085405 (2018).
- [12] B. Cohen-Stead, N. C. Costa, E. Khatami, and R. T. Scalettar, “Effect of strain on charge density wave order in the Holstein model,” *Phys. Rev. B* **100**, 045125 (2019).
- [13] Zi-Xiang Li, Marvin L. Cohen, and Dung-Hai Lee, “Enhancement of superconductivity by frustrating the charge order,” *Phys. Rev. B* **100**, 245105 (2019).
- [14] Chunhan Feng and Richard T. Scalettar, “Interplay of flat electronic bands with Holstein phonons,” *Phys. Rev. B* **102**, 235152 (2020).
- [15] B. Nosarzewski, E. W. Huang, Philip M. Dee, I. Esterlis, B. Moritz, S. A. Kivelson, S. Johnston, and T. P. Devereaux, “Superconductivity, charge density waves, and bipolarons in the Holstein model,” *Phys. Rev. B* **103**, 235156 (2021).
- [16] B. Xiao, N. C. Costa, E. Khatami, G. G. Batrouni, and R. T. Scalettar, “Charge density wave and superconductivity in the disordered Holstein model,” *Phys. Rev. B* **103**, L060501 (2021).
- [17] Owen Bradley, George G. Batrouni, and Richard T. Scalettar, “Superconductivity and charge density wave order in the two-dimensional Holstein model,” *Phys. Rev. B* **103**, 235104 (2021).
- [18] Philip M Dee, Jennifer Coulter, Kevin G Kleiner, and Steven Johnston, “Relative importance of nonlinear electron-phonon coupling and vertex corrections in the Holstein model,” *Communications Physics* **3**, 1–7 (2020).
- [19] H.G. Keiss, “Conjugated Conducting Polymers,” *Springer-Verlag Berlin* (1992).
- [20] T. Ishiguro and K. Yamaji, “Organic Superconductors,” *Springer-Verlag Berlin* (1990).
- [21] H. Toftlund and O. Simonsen, “Preparation and Structure of a New Kind of an Extended Partially Oxidized Linear Chain Compound- Catena-(Mu-Bromo)Bis((1R,2R)-Cyclohexanediamine)Nickel(2.77) Bromide,” *Inorg. Chem.* **23**, 4261 (1984).
- [22] Masashi Hase, Ichiro Terasaki, and Kunimitsu Uchinokura, “Observation of the spin-Peierls transition in linear Cu^{2+} (spin-1/2) chains in an inorganic compound CuGeO_3 ,” *Phys. Rev. Lett.* **70**, 3651–3654 (1993).
- [23] R. T. Scalettar, N. E. Bickers, and D. J. Scalapino, “Competition of Pairing and Peierls-CDW Correlations in a 2-D Electron-Phonon Model,” *Phys. Rev. B* **40**,

- 197–200 (1989).
- [24] W Koller, D Meyer, Y Ōno, and AC Hewson, “First-and second-order phase transitions in the Holstein-Hubbard model,” *EPL (Europhysics Letters)* **66**, 559 (2004).
- [25] Philipp Werner and Andrew J Millis, “Efficient dynamical mean field simulation of the Holstein-Hubbard model,” *Phys. Rev. Lett.* **99**, 146404 (2007).
- [26] H. Fehske, G. Hager, and E. Jeckelmann, “Metallicity in the half-filled Holstein-Hubbard model,” *EPL (Europhysics Letters)* **84**, 57001 (2008).
- [27] S. Johnston, E. A. Nowadnick, Y. F. Kung, B. Moritz, R. T. Scalettar, and T. P. Devereaux, “Determinant quantum Monte Carlo study of the two-dimensional single-band Hubbard-Holstein model,” *Phys. Rev. B* **87**, 235133 (2013).
- [28] Yao Wang, Ilya Esterlis, Tao Shi, J. Ignacio Cirac, and Eugene Demler, “Zero-temperature phases of the two-dimensional Hubbard-Holstein model: A non-Gaussian exact diagonalization study,” *Phys. Rev. Research* **2**, 043258 (2020).
- [29] Natanael C. Costa, Kazuhiro Seki, Seiji Yunoki, and Sandro Sorella, “Phase diagram of the two-dimensional Hubbard-Holstein model,” *Communications Physics* **3**, 1–6 (2020).
- [30] Zhaoyu Han, Steven A Kivelson, and Hong Yao, “Strong coupling limit of the Holstein-Hubbard model,” *Phys. Rev. Lett.* **125**, 167001 (2020).
- [31] Bo Xing, Wei-Ting Chiu, Dario Poletti, R. T. Scalettar, and George Batrouni, “Quantum Monte Carlo Simulations of the 2D Su-Schrieffer-Heeger Model,” *Phys. Rev. Lett.* **126**, 017601 (2021).
- [32] Xun Cai, Zi-Xiang Li, and Hong Yao, “Antiferromagnetism induced by electron-phonon-coupling,” (2021), [arXiv:2102.05060 \[cond-mat.str-el\]](https://arxiv.org/abs/2102.05060).
- [33] Anika Goetz, Stefan Beyl, Martin Hohenadler, and Fakher F. Assaad, “Langevin dynamics simulations of the two-dimensional Su-Schrieffer-Heeger model,” (2021), [arXiv:2102.08899 \[cond-mat.str-el\]](https://arxiv.org/abs/2102.08899).
- [34] John Sous, Monodeep Chakraborty, Roman V. Krems, and Mona Berciu, “Light Bipolarons Stabilized by Peierls Electron-Phonon Coupling,” *Phys. Rev. Lett.* **121**, 247001 (2018).
- [35] R. Blankenbecler, D. J. Scalapino, and R. L. Sugar, “Monte Carlo calculations of coupled boson-fermion systems. I,” *Phys. Rev. D* **24**, 2278–2286 (1981).
- [36] R. M. Noack, D. J. Scalapino, and R. T. Scalettar, “CDW and Pairing Susceptibilities in a Two Dimensional Electron-Phonon Model,” *Phys. Rev. Lett.* **66**, 778–781 (1991).
- [37] G. G. Batrouni and Richard T. Scalettar, “Langevin Simulations of a Long Range Electron Phonon Model,” *Phys. Rev. B* **99**, 035114 (2019).
- [38] R. L. Stratonovich, “On a Method of Calculating Quantum Distribution Functions,” *Soviet Physics Doklady* **2**, 416 (1957).
- [39] J. Hubbard, “Calculation of Partition Functions,” *Phys. Rev. Lett.* **3**, 77–78 (1959).
- [40] JE Hirsch and S Tang, “Antiferromagnetism in the two-dimensional Hubbard model,” *Phys. Rev. Lett.* **62**, 591 (1989).
- [41] S. R. White, D. J. Scalapino, R. L. Sugar, E. Y. Loh, J. E. Gubernatis, and R. T. Scalettar, “Numerical study of the two-dimensional Hubbard model,” *Phys. Rev. B* **40**, 506–516 (1989).
- [42] See Supplementary Material.
- [43] SR White, DJ Scalapino, RL Sugar, NE Bickers, and RT Scalettar, “Attractive and repulsive pairing interaction vertices for the two-dimensional Hubbard model,” *Phys. Rev. B* **39**, 839 (1989).
- [44] Th Pruschke and Robert Zitzler, “From Slater to Mott–Heisenberg physics: the antiferromagnetic phase of the Hubbard model,” *Journal of Physics: Condensed Matter* **15**, 7867 (2003).
- [45] Marcin Raczkowski, Fakher F Assaad, and Masatoshi Imada, “Local moments versus itinerant antiferromagnetism: Magnetic phase diagram and spectral properties of the anisotropic square lattice Hubbard model,” *Phys. Rev. B* **103**, 125137 (2021).
- [46] Chao Zhang, Nikolay V. Prokof’ev, and Boris V. Svistunov, “Bond Bipolarons: Sign-free Monte Carlo Approach,” (2021), [arXiv:2108.06725 \[cond-mat.supr-con\]](https://arxiv.org/abs/2108.06725).
- [47] <https://www.nscg.sg> .

Supplemental Material

In these Supplemental Materials we provide details concerning (a): An approximate treatment of the SSHH model in terms of a pure Hubbard Hamiltonian with a renormalized U_{eff} ; (b): The BOW Structure Factor with $U = 4, g = 1.5$; $U = 4, 15$ at $g = 1.0$ for $\beta = 16, L = 12$ system; (c): Scaling of the antiferromagnetic structure factor and, finally, (d): Structure factors at several different temperatures.

(a) Effective Hubbard Hamiltonian: In the Holstein model, where the phonons couple to the local charge density $H_{\text{el-ph}} = \lambda \sum_i \hat{X}_i n_i$, one can integrate out the phonon degrees of freedom in the anti-adiabatic limit (i.e. ignoring the phonon kinetic energy $\hat{P}^2/2M$ term). The result is an on-site attraction $U_{\text{eff}} = -\lambda^2/\omega_0^2$. As a consequence, the physics of the Hubbard-Holstein model at weak λ can be qualitatively interpreted in terms of a reduced on-site repulsion $U - \lambda^2/\omega_0^2$.

If one integrates out the SSH (bond) phonons on a two site dimer, the resulting effective electron-only Hamiltonian has a renormalized U , but also additional inter-site terms. Nevertheless, one can still ask the extent to which the SSHH model considered here can be quantitatively modeled simply by a renormalized U . We analyze this issue as follows: We first take data for the double occupancy $D = \langle n_{i\uparrow} n_{i\downarrow} \rangle$ both for the SSHH model at fixed $U = 4$ and varying g and for the pure Hubbard model at varying U . For each g , We define $U_{\text{eff}}(g)$ to be the value of U in the pure Hubbard case which gives the same D for the SSHH model. The result is given in the inset of panel (a) in Fig. S1.

Next we compare the values of *other* observables between SSHH at $U = 4$ and varying g with pure Hubbard at U_{eff} . By construction, the values for D match perfectly. Fig. S1(a,b) gives the results for the antiferromagnetic structure factor S_{AF} and kinetic energy $\langle K \rangle$ respectively. For S_{AF} the agreement between the actual SSHH data and the effective model is remarkable- the results match to within a few error bars across the complete range of g . Perhaps not surprisingly, the SSHH model captures the more abrupt change in S_{AF} at the AF-BOW phase transition than the effective model, which has no such transition.

The kinetic energy agreement is less good quantitatively, but still quite accurate qualitatively for small g . The effective model of course cannot capture the reduction in the magnitude of the kinetic energy at large g which occurs upon entry into the BOW phase. It is also observed in Fig. S1(b) that the kinetic energy of the SSHH model remains more constant for small g than does the kinetic energy of the effective model, an effect reminiscent of the appearance of weak g AF regime discussed in the main text. The effective model gives a rough context in which to understand the suppression

of magnetism by g . The resulting accuracy of panel (a) of Figure S1 is of additional interest: it is not obvious that adjusting U to get a match for a local observable like double occupancy would also give a good match for intersite magnetic correlations.

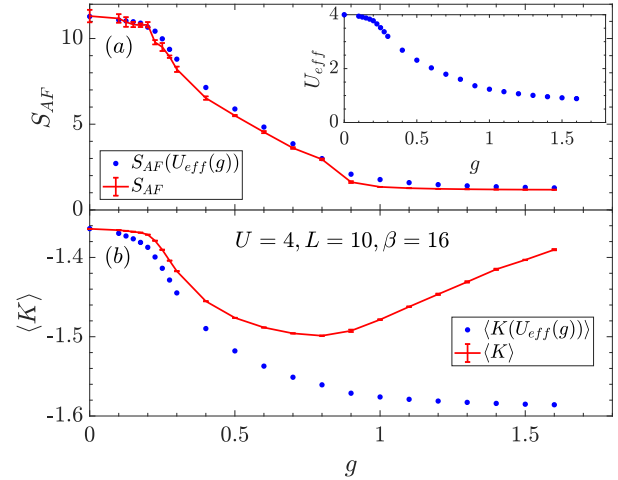


FIG. S1. Inset in panel (a): In SSHH model, when $U = 4, \beta = 16$ on a $L \times L = 10 \times 10$ square lattice, for each g , we define U_{eff} as the onsite electron repulsion in the pure Hubbard model which gives the same double occupancy D . (a) AF structure factor (b) Electron Kinetic energy given in SSHH model (red curve), for $U = 4$, varying $g, \beta = 16$ on a $L \times L = 10 \times 10$ square lattice and in pure Hubbard model (blue dot) when $\beta = 16$ on a $L \times L = 10 \times 10$ with U_{eff} defined in Fig. S1 (a) inset. Two curves are in reasonable agreement at relatively small g , while the discrepancy at large g is because BOW phase can not be captured by the pure Hubbard model.

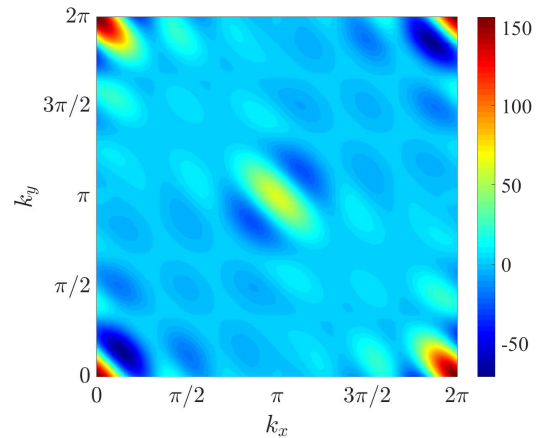


FIG. S2. Bond ordered wave structure factor, $S_{K_x}(k_x, k_y)$ as a function of momentum k_x, k_y for $U = 4, g = 1.5, \beta = 16, L = 12$.

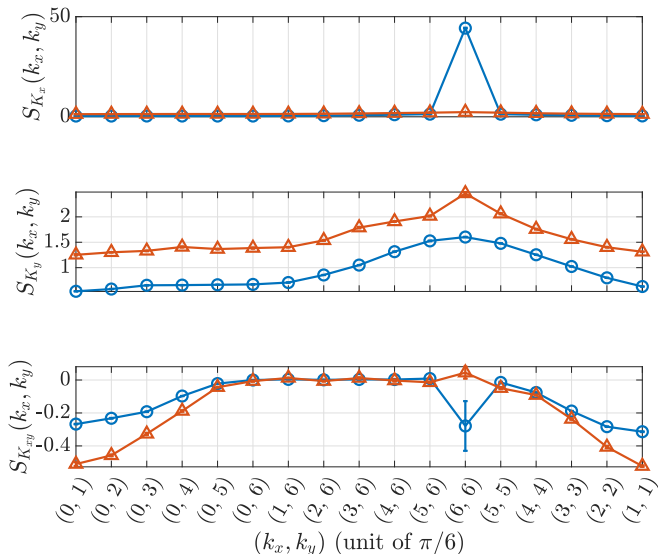


FIG. S3. Bond ordered wave structure factor, S_{K_x} (top), S_{K_y} (center), $S_{K_{xy}}$ (bottom) for different (k_x, k_y) momenta. The blue and red curves correspond to $U = 4$ and $U = 15$ respectively. The other system parameters are $g = 1.0$, $\omega = 1$, $L = 12$, and $\beta = 16$.

(b) Bond ordered wave structure factor: For all simulations, we start with a phonon configuration that favors the development of XX bond ordered wave (BOW) pattern, i.e. (π, π) order of the x bonds. As noted in the main text, we have verified that for small lattices and high temperatures, correlation functions are independent of initial configuration, and evolve to a consistent long time state. In addition, for all lattice sizes and temperatures, BOW melts rapidly when it is not supported by the parameters of the simulation. Thus our choice of starting configuration serves only to minimize long equilibration times in the BOW phase, and does not affect our determination of the phase diagram. Fig. S2 shows the BOW structure factor $S_{K_x}(k_x, k_y)$, the Fourier transform of bond-bond kinetic energy correlations in real space, as a function of momenta k_x and k_y . Besides a large value at $(k_x, k_y) = (0, 0)$, which is actually the sum of all spatial correlations, a clear peak is observed at $(k_x, k_y) = (\pi, \pi)$ for $U = 4, g = 1.5, L = 12, \beta = 16$ system (in BOW phase). In Fig. S3, we show the BOW structure factors for different directions and momenta when the system is in the BOW phase, i.e. $U = 4, g = 1.0$. For all S_{K_x}, S_{K_y} and $S_{K_{xy}}$, we find a peak only at $S_{K_x}(\pi, \pi)$. It is worth pointing out that, despite the large error bar at $S_{K_{xy}}(\pi, \pi)$, the negligible magnitude of its structure factor suggests that there is no notable structure in the XY direction. When the system is not in the BOW phase, i.e. $U = 15, g = 1.0$, the BOW structure factors for all three directions become negligible.

(c) Antiferromagnetic structure factor: In Fig S4, we

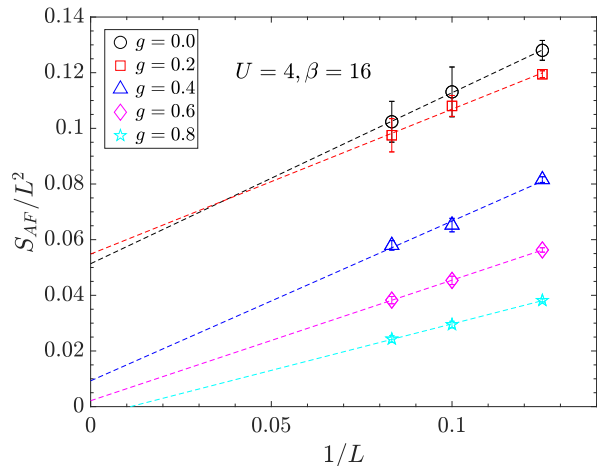


FIG. S4. Finite size scaling of the antiferromagnetic structure factor, S_{AF}/L^2 , for $g = 0, 0.2, 0.4, 0.6, 0.8$. The dotted lines are extrapolated from the simulations data. For all results shown in this panel, $U = 4, \beta = 16$.

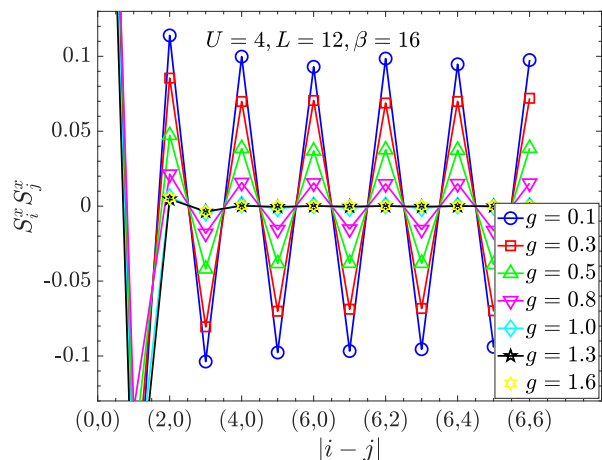


FIG. S5. Spin-spin correlation, $\langle S_i^x S_j^x \rangle$ versus spatial distance $|i - j|$ for various g .

perform finite size scaling (FSS) of the antiferromagnetic structure factor, S_{AF}/L^2 and show that the antiferromagnetic (AF) structure is present in the thermodynamic limit for both AF regions. At $U = 4, g = 0$, the system is in the AF phase. As g increases, S_{AF}/L^2 decreases in the thermodynamic limit. However, it is still finite and therefore indicative of the AF phase. At $g = 0.8$, we notice that FSS of S_{AF}/L^2 becomes less than zero. At the same time, the BOW structure factor, $S_{K_x}(\pi, \pi)$, rises sharply to a finite value, indicating the direct transition from the AF phase to the BOW phase.

In Fig. S5, the AF correlation function in real space gives similar conclusions. The oscillation of the AF correlation function, which does not decay with the

spatial distance, gives evidence to the presence of the AF phase. As g increases, the magnitude of this oscillation decreases. The strong oscillation of the AF correlation function for $g < 0.8$, and the absence of BOW correlation, show that in this parameter region the system is AF.

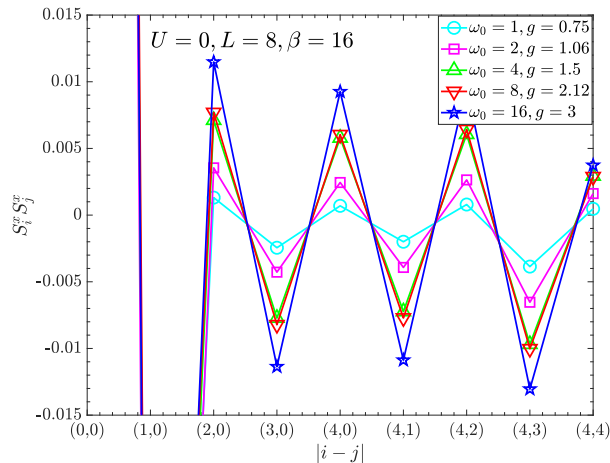


FIG. S6. Spin-spin correlation, $\langle S_i^x S_j^x \rangle$ versus spatial distance $|i - j|$ for several phonon frequencies, ω_0 , for the pure SSH model on an 8×8 square lattice. Increasing ω_0 at fixed g^2/ω_0 enhances AF order.

We also verify that for the pure SSH model ($U = 0$), when $g \lesssim g_c$, long range AF order exists at low temperature ($\beta = 16$). The spin-spin correlation as a function of lattice site separation is shown in Fig. S6. As ω_0 increases with g^2/ω_0 (which is proportional to the spin exchange strength in the anti-adiabatic limit) fixed, the AF order is strengthened, which is consistent with the conclusion in [32, 33]

(d) Structure factors at several different temperatures

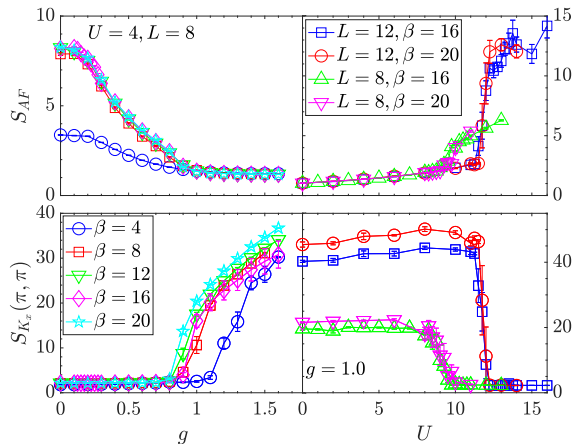


FIG. S7. Left panels: AF and BOW structure factors vs. electron-phonon coupling g for a fixed $U = 4$, at several different temperatures $\beta = 4, 8, 12, 16, 20$. Right panels: AF and BOW structure factors vs. onsite Coulomb interaction U for a fixed $g = 1.0$, $\beta = 16, 20$ on 8×8 and 12×12 lattices. Both panels indicate $\beta = 16$ is low enough to capture the ground state physics for the SSHH model.

In the left panels of Fig. S7, the AF and BOW structure factors are plotted as functions of electron-phonon coupling strength g for a fixed $U = 4$ on a 8×8 square lattice. The curves almost overlap when $\beta \gtrsim 8$, indicating the temperature we use ($\beta = 16$) in the main text is low enough to capture the ground state physics. Similarly, the right panels are structure factors S_{AF} and $S_{K_x}(\pi, \pi)$ vs. U . Although their magnitudes at $\beta = 20$ in the ordered phase are slightly larger than those given by $\beta = 16$, the transition point given by them coincide for both $L = 8$ and $L = 12$ lattices respectively. There is some finite size effect going from $L = 8$ to $L = 12$ in both Fig. S7 and Fig. 1 but there is no such effect between $L = 10$ and $L = 12$.